Control-relevant Modelling and Linear Analysis of Instabilities in Oxy-fuel Combustion

Dagfinn Snarheim, Lars Imsland and Bjarne A. Foss

***Abstract*— Semi-closed gas turbine cycles based on oxy-fuel combustion have been proposed as an alternative to conventional gas turbine cycles for achieving CO_2-capture for CO_2 sequestration purposes. While combustion instabilities is a problem in modern conventional gas turbines in general, recent experimental results indicate that such instabilites also occur in oxy-fuel combustion. For conventional combustion processes, model based controllers have been successful at suppressing thermoacoustic instabilities. As a first step towards achieving the same for oxy-fuel combustion, we develop a control relevant model of oxy-fuel combustion. In oxy-fuel combustion CO_2 is used as working medium instead of air. From a control point of view, this gives an extra degree of freedom (compared to conventional combustion control). Analysis on the developed model show that secondary injection of CO_2 close to the flame is probably a better manipulated variable than fuel-injection, which has been a popular choice for control in conventional combustion processes.**

I. Introduction

Gas turbines are widely used for power production from gaseous fossil fuels. Although gas turbine engines are relatively clean burning, there is inevitably a production of CO_2 from combustion of fossil fuels. Thus, with today's increasing concern about global warming and climate change, there is an incentive to investigate gas turbine processes with CO_2 capture.

One attractive concept for this is the semi-closed gas turbine cycles using CO_2 as working medium. This process has been studied in e.g [1], [2], [3]. Central in the concept is that combustion of natural gas together with a mixture of CO_2 (as gas turbine working medium) and O_2 leaves the exhaust consisting mainly of water and CO_2. The water can be removed using a condenser, and we are left with (almost) pure CO_2, of which most is recycled for use as working medium, while to avoid accumulation, some must be removed from the cycle. The removed CO_2 must be compressed for long term safe storage, to have the desired positive effect on the global warming (carbon sequestraion).

While overall process dynamics has been studied in [4], [5], in this paper, we concentrate on the dynamics of the combustion chamber. It is known that conventional gas turbine combustion chambers might exihibit detrimental instabilities under some operating conditions [6, e.g.]. Recent experimental work [7] indicates that similar instabilities also occur in oxy-fuel combustion, possibly even more severe than in the conventional case.

Dagfinn Snarheim and Bjarne A. Foss are with the Department of Engineering Cybernetics, Norwegian University of Science and Technology, N 7491 Trondheim, Norway. {Dagfinn.Snarheim,Bjarne.A.Foss}@itk.ntnu.no

L. Imsland is with SINTEF ICT, Applied Cybernetics, N 7465 Trondheim, Norway. Lars.Imsland@sintef.no

This gives a clear motivation for studying if it is possible to use active feedback control for alleviating these instabilities for oxyfuel combustion, as has been successfully done for conventional combustion [6]. This paper provides a first step in that direction: We will first develop a new linear low-order model, inspired from similar models for conventional combustion, for studying the dynamics that are at the root of the observed instabilities. Due to the fact that the number of control degrees of freedom is higher for oxyfuel combustion than for conventional combustion, we thereafter use the developed model to study which of the control degrees of freedom is more suitable for doing active feedback stabilization, and to give indications towards requirements for actuation devices.

The paper is briefly outlined as follows: In Section II we give som brief background on combustion instabilities in general, then we proceed to discuss the special case oxy-fuel combustion. The modelling of the process is presented in Section III, while Section IV looks at requirements for the input part of a control system to stabilize the plant. We end the paper with some concluding remarks.

II. Thermodynamic instabilities in oxy-fuel combustion

Thermodynamic instabilites have been recognized as a problem in combustion processes for a long time. These instabilities take the form of large pressure oscillations in the combustion chamber. That the coupling between unsteady heat release oscillations and acoustic pressure can be a driving mechanism for thermodynamic instabilities was identified as early as 1878 [8]. The heat release and acoustics are coupled in a feedback loop, and depending on the phase difference between the signals, the heat release either remove from or add energy to the pressure oscillations, the latter case making the system unstable. Obvious implications of these instabilities are vibration and mechanical stress that may lead to structural damage and system failure. Alleviating the oscillations might allow for better energy utilization and less pollutant emissions.

Modern (conventional) premixed gas turbines have to operate at very lean conditions due stringent requirements on NO_x emissions. These operating conditions make the gas turbines extra prone to instabilities, and is an important reason for all the attention active control of thermoacoustic instabilities has received recently. This is also reflected in the numerous publications within the field in recent years. Reviews on thermoacoustic instabilities and active control can be found in [6], [9], [10].

However, when it comes to oxy-fuel, the literature on instabilities is scarce. Experimental results on a laboratory scale combustor are published in [7]. They show that up to a certain threshold in oxidizer composition (the ratio between oxygen and carbone dioxide in the oxy-fuel mixture), the instability patterns are similar to what you find when burning fuel with air. Above this threshold the instabilities tends to grow even stronger. Figure 1 shows sound pressure level plots from these experiments. The unstable frequencies are easy to identify in the peaks. Due to the geometry in the experiment, there exists several acoustic modes that can be triggered. Which one is triggered depends on the operating conditions. This gives a clear incentive to investigate active control strategies for this type of combustion. Moreover, it also indicates that a good controller must be able to reduce pressure oscillations over a broad frequency range, possibly broader than for conventional combustion instabilities.

In oxy-fuel combustion it is possible to change the composition of the oxidizer (the ratio between O_2 and CO_2). Compared to conventional combustion in air, this is the equivalent of changing the ratio between nitrogen and oxygen, which generally is hard/expensive. The difference between plot b) and c) in Figure 1 indicates that the oxidizer composition is very important. From a control point of view, this means that for oxy-fuel there exists a new degree of freedom that can be used to stabilize the system. One focus of this paper is to model the effect of perturbations in oxidizer composition, and investigate the use of this variable for control. The extra degree of freedom is illustrated in Figure 2.

III. Modelling

In combustion processes there are several components that contribute to the overall dynamics. These include acoustics, fluid dynamics, transport processes, chemical kinetics, flame kinematics, heat transfer, feedline dynamics of the reactants, and atomization and vaporization dynamics. These components can couple with each other in various ways, and developing a detailed model of such a complex system is an extremely challenging task [6]. Moreover, such models are not well suited for controller design. For active control of conventional combustion, model-based controllers have proven to supress thermoacoustic instabilites better than empirical controllers. We expect the same to be true for oxy-fuel combustion. Thus there is a need for low order models of oxy-fuel combustion. A common approach that captures the most important dynamics is to model the acoustics and the heat release. A linear form of the wave equation is then used for the acoustics. For the heat release dynamics we will use a thin wrinkled flame model developed by [11]. This model where extended for perturpations in equivalence ratio by [12], and we will in the following extend it to perturbations in oxidizer ratio. An early version of the modelling herein can be found in [13].

The combustion chamber that we model is of length L and has a width D. As in [14] the burner consists of a perforated plate with n_f holes, each with a radius R. In each of these holes there is a flame at location x_f. Figure 3 shows a skecth of one such flame.

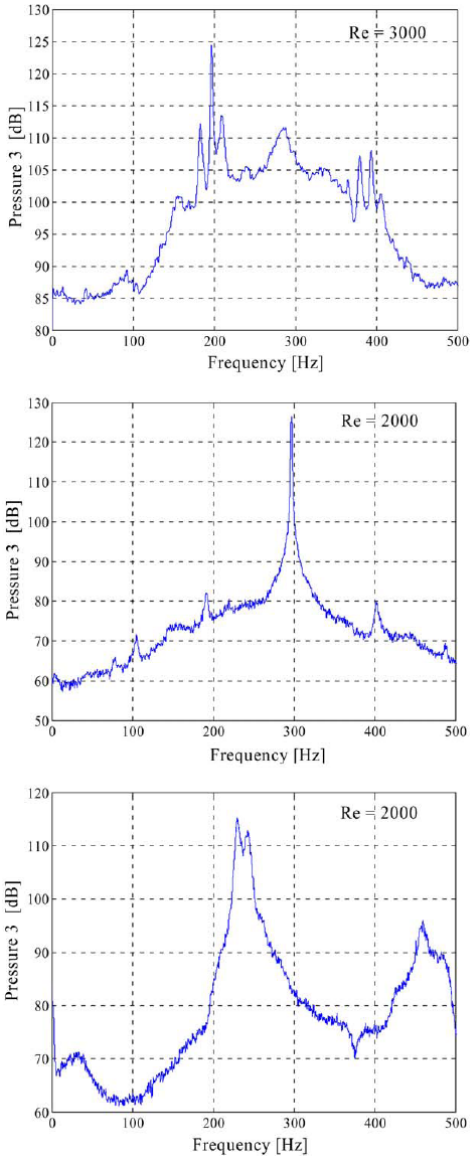

Fig. 1: Experimental results from oxy-fuel combustor. The triggered frequency and instability peak is dependant on operating conditions: a) $\lambda_{O_2} = 0.42$, $\phi = 0.9$, $\mathrm{Re} = 3000$; b) $\lambda_{O_2} = 0.41$, $\phi = 0.9$, $\mathrm{Re} = 2000$; c) $\lambda_{O_2} = 0.42$, $\mathrm{Re} = 2000$, $\phi = 0.9$. (from [7])

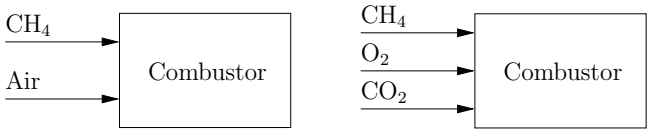

(a) Conventional combustion chamber

(b) Oxy-fuel combustion chamber

Fig. 2: Conceptual difference between a conventional combustion chamber and an oxy-fuel combustion chamber from a control point of view.

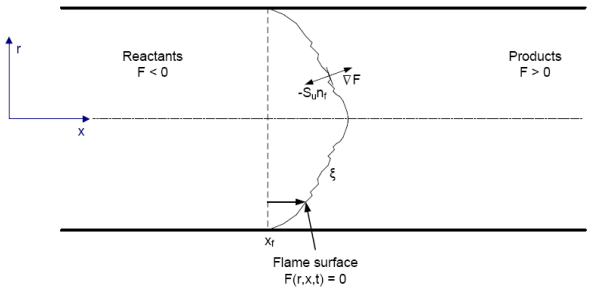

Fig. 3: The flame front in the combustion chamber.

One important difference between oxy-fuel combustion and conventional combustion is the possibility of changing the oxidizer composition. To describe the composition we define the oxidizer ratio as

$$\lambda_{O_2} = \frac{n_{O_2}}{n_{O_2} + n_{CO_2}}, \tag{1}$$

where n_x refers to the number of moles of component x. Together with equivalence ratio

$$\phi = \frac{\left(n_{fuel}/n_{O_2}\right)_{actual}}{\left(n_{fuel}/n_{O_2}\right)_{stoichiometric}} \tag{2}$$

and the total mass flow ($\dot{m}_{tot}$) we have full information of the mass flows of the different components.

A. Heat release

The starting point for the modelling is the the flame surface equation from [11] with modifications to take λ_{O_2} into account

$$\frac{\partial \xi}{\partial t} = u - v\frac{\partial \xi}{\partial r} - S_u\left(\phi, \lambda_{O_2}\right)\sqrt{1 + \left(\frac{\partial \xi}{\partial r}\right)^2},$$

where $\xi(r,t)$ is a single-valued function describing the axial displacement of the flamesurface, u is axial velocity, v is radial velocity and S_u is the laminar burning velocity. The different variables are illustrated in Figure 3. The area of the flame can be found by performing a surface integral of the variable ξ, and the heat release from the flame is assumed to be proportional to the flame area (A_f),

$$\begin{aligned} Q &= \rho_u\left(\phi, \lambda_{O_2}\right) S_u\left(\phi, \lambda_{O_2}\right) \Delta h_r\left(\phi, \lambda_{O_2}\right) A_f, \qquad (3)\\ A_f &= 2\pi \int_0^R r\sqrt{1 + \left(\frac{\partial \xi}{\partial r}\right)^2}\, dr. \end{aligned}$$

Here, ρ_u is the density of the unburnt mixture, Δh_r is the heat of reaction per unit mass of the mixture and R is the radius of the burner. So far the main difference from conventional combustion is that λ_{O_2} enters the equations through ρ_u, Δh_r and λ_{O_2}. We now proceed to extend the model in a similar way as in [12], with necessary modifications for λ_{O_2}.

We assume very small radial velocity and v is thus neglected. Also, ρ_u will not change much with perturbations in ϕ and λ_{O_2} and will be assumed constant. We denote mean values as $\bar{(\cdot)}$ and deviation value as $(\cdot)'$, and linearize around $\bar{u}$, $\bar{\phi}$, $\bar{\lambda}_{O_2}$ and $\bar{\xi}$, and get

$$\frac{\partial \xi'}{\partial t} = u' + \bar{S}_u\frac{\partial \xi'}{\partial r} + \frac{\partial \bar{\xi}}{\partial r}\left(\frac{\partial \bar{S}_u}{\partial \phi}\phi' + \frac{\partial \bar{S}_u}{\partial \lambda_{O_2}}\lambda'_{O_2}\right). \tag{4}$$

Note here that for brevity we use the notation $\frac{\partial \bar{S}_u}{\partial \phi}$ for $\left.\frac{\partial S_u}{\partial \phi}\right|_{\phi=\bar{\phi},\lambda_{O_2}=\bar{\lambda}_{O_2}}$. Similar notation is used throughout the document. The boundary and initial conditions for ξ' is

$$\xi'(R,t) = 0, \qquad \xi'(r,0) = 0.$$

Similarily, linearization of the heat release equation (3) gives

$$Q' = \bar{\kappa}\int_0^R \xi'(r,t)\, dr + d_1\phi' + d_2\lambda'_{O_2} \tag{5}$$

where

$$\bar{\kappa} = 2\pi\rho_u\bar{S}_u\Delta\bar{h}_r,$$

and

$$\begin{aligned} d_1 &= 2\pi\rho_u\left(\bar{S}_u\frac{\partial \Delta\bar{h}_r}{\partial \phi} + \Delta\bar{h}_r\frac{\partial \bar{S}_u}{\partial \phi}\right)\left(\int_0^R \bar{\xi}(r)\, dr\right),\\ d_2 &= 2\pi\rho_u\left(\bar{S}_u\frac{\partial \Delta\bar{h}_r}{\partial \lambda_{O_2}} + \Delta\bar{h}_r\frac{\partial \bar{S}_u}{\partial \lambda_{O_2}}\right)\left(\int_0^R \bar{\xi}(r)\, dr\right). \end{aligned}$$

Differentiatiating equation (5) and inserting equation (4) gives

$$\begin{aligned} \dot{Q}' = \bar{\kappa}\int_0^R u' + \bar{S}_u\frac{\partial \xi'}{\partial r} + \\ \frac{\partial \bar{\xi}}{\partial r}\left(\frac{\partial \bar{S}_u}{\partial \phi}\phi' + \frac{\partial \bar{S}_u}{\partial \lambda_{O_2}}\lambda'_{O_2}\right) dr + d_1\dot{\phi}' + d_2\dot{\lambda}'_{O_2} \end{aligned} \tag{6}$$

which is integrated over r as

$$\dot{Q}' = \bar{\kappa}\left(Ru' - \bar{S}_u\xi'(0,t) + d_5\phi' + d_6\lambda'_{O_2}\right) + d_1\dot{\phi}' + d_2\dot{\lambda}_{O_2} \tag{7}$$

where

$$d_5 = -\xi(0)\frac{\partial \bar{S}_u}{\partial \phi}, \qquad d_6 = -\xi(0)\frac{\partial \bar{S}_u}{\partial \lambda_{O_2}}.$$

To proceed we need an expression for $\xi'(0,t)$. This is found by taking the Laplace transform of equation (4) and solving the resulting differential equation in r

$$\begin{aligned} \xi'(r,s) = \left(\frac{u'}{s} + \frac{\partial \bar{\xi}}{\partial r}\left(\frac{\partial \bar{S}_u}{\partial \phi}\frac{\phi'}{s} + \frac{\partial \bar{S}_u}{\partial \lambda_{O_2}}\frac{\lambda'_{O_2}}{s}\right)\right) \\ \times\left(1 - e^{-(R-r)\frac{s}{\bar{S}_u}}\right). \end{aligned} \tag{8}$$

Taking the inverse Laplace transform gives

$$\begin{aligned} \xi'(r,t) = \int_{t-\tau_r}^t u'(\tau)\, d\tau + \frac{\partial \bar{\xi}}{\partial r}\frac{\partial \bar{S}_u}{\partial \phi}\int_{t-\tau_r}^t \phi'(\tau)\, d\tau \\ + \frac{\partial \bar{\xi}}{\partial r}\frac{\partial \bar{S}_u}{\partial \lambda_{O_2}}\int_{t-\tau_r}^t \lambda_{O_2}(\tau)\, d\tau \end{aligned} \tag{9}$$

where $\tau_r = \frac{R-r}{\bar{S}_u}$.

As in [14] we approximate

$$\int_{t-\tau_r}^{t} u'(\tau)\,d\tau \approx \frac{R-r}{\bar{S}_u}u' \tag{10}$$

and in a similar way

$$\int_{t-\tau_r}^{t} \phi'(\tau)\,d\tau \approx \frac{R-r}{\bar{S}_u}\phi', \tag{11}$$
$$\int_{t-\tau_r}^{t} \lambda'_{O_2}(\tau)\,d\tau \approx \frac{R-r}{\bar{S}_u}\lambda'_{O_2}.$$

Using these approximations in equation (9), then inserting in equation (5) and solving the resulting integral gives

$$Q' = \frac{\kappa R}{2}\frac{R}{\bar{S}_u}u' + \left(d_1 + \frac{\kappa R}{2\bar{S}_u}d_5\right)\phi' + \left(d_2 + \frac{\bar{\kappa}R}{2\bar{S}_u}d_6\right)\lambda'_{O_2} \tag{12}$$

If we now evaluate $\xi'(0,t)$ using the approximations in equation (10) and (11) we get

$$\xi'(0,t) = \frac{R}{\bar{S}_u}u' + d_3\frac{R}{\bar{S}_u}\phi' + d_4\frac{R}{\bar{S}_u}\lambda'_{O_2}. \tag{13}$$

We then get an expression for u' from equation (12) and insert it in equation (13) resulting in

$$\xi'(0,t) = \frac{2Q'}{\kappa R} - \frac{2}{\kappa R}\left(d_1 + \frac{\kappa R}{2\bar{S}_u}d_5 - \frac{\kappa R^2}{2\bar{S}_u}d_3\right)\phi' - \frac{2}{\kappa R}\left(d_2 + \frac{\kappa R}{2\bar{S}_u}d_6 - \frac{\kappa R^2}{2\bar{S}_u}d_4\right)\lambda'_{O_2}. \tag{14}$$

Now this equation can be inserted into equation (7) and we arrive at

$$\dot{Q}' + \frac{2\bar{S}_u}{R}Q' = \kappa R u' - \left(\frac{2\bar{S}_u}{R}d_1 - \frac{\kappa R}{\bar{S}_u}d_3\right)\phi' - \left(\frac{2\bar{S}_u}{R}d_2 - \frac{\kappa R}{\bar{S}_u}d_4\right)\lambda'_{O_2} + d_1\dot{\phi}' + d_2\dot{\lambda}_{O_2}. \tag{15}$$

B. Acoustics

We consider a tube with length L and use a one-dimensional wave equation to describe the pressure fluctuations $p' = p - \bar{p}$.

$$\frac{\partial^2 p'}{\partial t^2} - \bar{c}^2\frac{\partial^2 p'}{\partial x^2} = (\gamma-1)\frac{\partial q'}{\partial t}(x,t),$$

where p is pressure, q is the heat release per area $\left(q = \frac{Q}{\pi(D/2)^2}n_f\right)$, c is the speed of sound and γ is the specific heat ratio. The pressure oscillations are coupled to velocity perturbations by

$$\frac{\partial p'}{\partial t} + \gamma\bar{p}\frac{\partial u'}{\partial x} = (\gamma-1)\,q'. \tag{16}$$

The combustion chamber is closed at the inlet and open at the outlet, resulting in the following boundary conditions

$$p'(L,t) = 0,$$
$$u'(0,t) = 0.$$

The wave equation is discretized using the Galerkin expansion

$$p'(x,t) = \bar{p}\sum_{i=1}^{n}\psi_i(x)\eta_i(t),$$

where $\psi_i(x)$ and $\eta_i(t)$ are modal shape and amplitude, $\psi_i(x) = \cos(k_i x)$. Using this expansion within the wave-equation and integrating over the combustor length (L) gives as in [14]

$$\ddot{\eta}_i + \omega_i^2\eta_\iota = \tilde{b}_i\dot{q}'_f$$

where $\tilde{b}_i = \gamma a_0\psi(x_f)/E$, $E = \int_0^L \psi_i^2(x)\,dx$, $a_0 = \frac{\gamma-1}{\gamma\bar{p}}$ and $\omega_i = k_i\bar{c}$. As in [12] we also add a damping term ζ to account for heat and friction losses within the combustor

$$\ddot{\eta}_i + 2\zeta\omega_i\dot{\eta}_i + \omega_i^2\eta_i = \tilde{b}_i\dot{q}'_f.$$

In a similar way the Galerkin expansion is used on equation (16). Integration over the combustor length L then gives

$$u' = \sum_{i=1}^{n}\tilde{c}_i\dot{\eta}_i + \theta a_0 q' + u_c,$$

where $\tilde{c}_i = \frac{1}{\gamma k_i^2}\frac{d\psi_i}{dx}(x_f)$, $a_0 = (\gamma-1)/\gamma\bar{p}$ and θ represents the effect of the velocity ahead and behind the flame on q' and u_c is the velocity added by potential secondary injectors. We assume perfect mixing of the components in the unburnt mixture, and thus the pressure oscillations have no effect on the equivalance ratio (ϕ) and the oxidizer ratio (λ_{O_2}). Inserting the velocity relation into equation (15) gives

$$\dot{Q}' + \left(\frac{2\bar{S}_u}{R} - \kappa R\theta a_0\frac{n_f}{A_c}\right)Q' = \kappa R\sum_{i=1}^{n}\tilde{c}_i\dot{\eta}_i + \kappa R u_c - \left(\frac{2\bar{S}_u}{R}d_1 - \frac{\kappa R}{\bar{S}_u}d_3\right)\phi' - \left(\frac{2\bar{S}_u}{R}d_2 - \frac{\kappa R}{\bar{S}_u}d_4\right)\lambda'_{O_2} + d_1\dot{\phi}' + d_2\dot{\lambda}_{O_2}. \tag{17}$$

As the flame is nearly conical, the slope at the tip will be close to zero. As d_3 and d_4 are proportional to the derivative of the mean flameshape at $r = 0$, they are close to zero and can be neglected. The resulting heatrelase model then becomes

$$\dot{Q}' + \left(\frac{2\bar{S}_u}{R} - \kappa R\theta a_0\frac{n_f}{A_c}\right)Q' = \kappa R\sum_{i=1}^{n}\tilde{c}_i\dot{\eta}_i + \kappa R u_c - \frac{2\bar{S}_u}{R}d_1\phi' - \frac{2\bar{S}_u}{R}d_2\lambda'_{O_2} + d_1\dot{\phi}' + d_2\dot{\lambda}_{O_2}. \tag{18}$$

C. Actuators

In this paper we study the use of secondary injectors to control the system. We choose to not model the dynamics in the actuators. This in spite of that the dynamics in the actuators are important because their bandwith will typically be close to the unstable frequencies they are used to stabilize. However, the actuator dynamics will have similar influence on all the inputs, and will not be important in the choice of manipulated variable for the system. The actuator dynamics will also be dependent on the specific valve chosen to actuate the system. Instead we use the model to analyse which requirements there will be on the actuators to be able to stabilize the system (see Section IV).

However, we do need linear relations between ϕ', λ'_{O_2} and the different mass flows (w). Starting with the definition of λ_{O_2} and ϕ (equation (1) and (2)), linearization around the operation point gives

$$\phi' = \frac{1}{\bar{w}_{O_2}\alpha_0} w'_{CH_4} - \frac{\bar{\phi}}{\bar{w}_{O_2}} w'_{O_2} \tag{19}$$
$$\lambda'_{O_2} = \frac{1-\bar{\lambda}_{O_2}}{\alpha_1 MW_{O_2}} w'_{O_2} - \frac{\bar{\lambda}_{O_2}}{\alpha_1 MW_{CO_2}} w'_{CO_2}.$$

where $\alpha_0 = \left(\frac{w_{CH_4}}{w_{O_2}}\right)_{\text{stoichiometric}}$ and $\alpha_1 = \frac{\bar{w}_{O_2}}{MW_{O_2}} + \frac{\bar{w}_{CO_2}}{MW_{CO_2}}$ and MW_x is the molecular weight of compononent x. Then remembering that we have n_f holes with radius R, we get the following equation for u_c

$$u_c = \frac{\left(w'_{CH_4} + w'_{O_2} + w'_{CO_2}\right)}{\rho_u n_f \pi R^2}.$$

There will also be a transport delay (τ_c) assosciated with convection from the injector to the burning zone, $\tau_c = L_c/\bar{u}$, where L_c is the distance from the injector to the burning zone.

D. Heat of reaction and flame speed

The heat of reaction is the maximum heat release per kg fuel that can occur within the combustor. We calculate it using the lower heating value (LHV) for methane, $\Delta h_r = LHV_{CH_4} m_{CH_4}/m_{tot}$. We can express Δh_r as a function of ϕ and λ_{O_2},

$$\Delta h_r = LHV_{CH_4} \times \frac{\phi\lambda_{O_2} MW_{CH_4}}{2\lambda_{O_2} MW_{O_2} + 2MW_{CO_2}(1-\lambda_{O_2}) + \phi\lambda_{O_2} MW_{CH_4}}.$$

We can now calculate the partial derivates of Δh_r that enters the model equations

$$\frac{\partial \Delta h_r}{\partial \phi} = LHV_{CH_4} \times \frac{2\lambda_{O_2} MW_{CH_4}\left(MW_{CO_2}(1-\lambda_{O_2}) + \lambda_{O_2} MW_{O_2}\right)}{\left(2\lambda_{O_2} MW_{O_2} + 2MW_{CO_2}(1-\lambda_{O_2}) + \phi\lambda_{O_2} MW_{CH_4}\right)^2}$$

$$\frac{\partial \Delta h_r}{\partial \lambda_{O_2}} = LHV_{CH_4} \times \frac{2\phi MW_{CH_4} MW_{CO_2}}{\left(2\lambda_{O_2} MW_{O_2} + 2MW_{CO_2}(1-\lambda_{O_2}) + \phi\lambda_{O_2} MW_{CH_4}\right)^2}.$$

As these equations only enter the model as constants, it is not necessary to linearize them.

It seems difficult to derive analytical expressions for S_u that uses thermodynamic property tables. We chose instead to perform equilibrium calculations using a methane mechanism (GRI 3.0) to generate a lookup table for S_u. Curvefitting of this data was then used as a model. Figure 4 shows this relation, were the $\phi = 1$ line has been published in [7]. Note that S_u varies significantly more with λ_{O_2} than with ϕ. In a conventional combustion process, where λ_{O_2} is 21%, and you can only change ϕ, S_u is close to constant. On the other hand, for oxy-fuel combustion S_u can vary a lot,

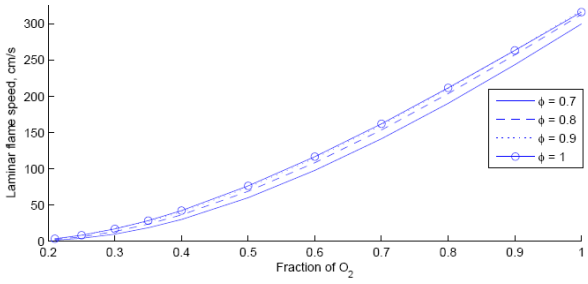

Fig. 4: The laminar flames speed (S_u) as a function of equivalence ratio and oxidizer ratio.

and we expect this to have an impact on the controllability of the process.

Based on the curvefits we get the following equations for the partial derivatives of S_u.

$$\frac{\partial S_u}{\partial \phi} = 1.7923\lambda_{O_2}^2 - 0.3780\phi\lambda_{O_2} + 0.43\lambda_{O_2} - 0.1930$$
$$\frac{\partial S_u}{\partial \lambda_{O_2}} = 3.5846\phi\lambda_{O_2} - 0.1890\phi^2 + 0.43\phi + 2.837\lambda_{O_2}$$

E. Implementation and model validity

The complete model was implemented in Simulink using two modes for the acoustics. We kept the inputs on velocity form (du/dt), resulting in the following input vector $u = \begin{bmatrix} \dot{u}'_c & \dot{\phi} & \dot{\lambda}_{O_2} & \dot{w}_{CH_4} & \dot{w}_{O_2} & \dot{w}_{CO_2} \end{bmatrix}$. We used a similar geometry as in [14]. The length of the combustion chamber $L = 0.49\,\text{m}$, the width is $D = 0.04\,\text{m}$ and the flame is located at $x_f = 0.24\,\text{m}$. The chamber consists of $n_f = 80$ burners, each with a radius $R = 0.75\,\text{mm}$. The cost of oxygen implies operation at close to stoichiometric conditions [7]. Thus we choose to operate the system near $\phi = 1$ and $\lambda_{O_2} = 0.35$. Based on this we can calculate $\bar{c} = 310.6$, $\rho_u = 1.47\,\text{kg}/\,\text{m}^3$ and $\Delta\bar{h}_r = 3.315MJ/\,\text{kg}$. We use $\bar{p} = 10^5\,\text{Pa}$, $\gamma = 1.4$, , $\theta = 0.5$ and $\zeta = 0.01$.

As the literature on dynamics in oxy-fuel combustion is scarce, it is difficult to find data for validation of the model. Due to the need to keep the model simple (low order) and because we use a linear model, there are certain effects that the model cannot capture. Figure 5 shows the response of the uncontrolled system to a disturbance in the oxidizer ratio λ_{O_2}. The system is clearly unstable. In real combustion processes, the pressure oscillations will enter a limit cycle, an effect that this model cannot capture. If we look back at Figure 1, we cannot do similar sound pressure level calculations based on the model output. To calculate the sound pressure level only makes sense when the pressure oscillations are limited by a limit cycle. We can, however, use fourier transforms to calculate the frequency of the oscillations. In Figure 5 the system oscillates with a frequency equal to $\omega_2 \approx 3000\,\text{rad}\,/\,\text{s}$, indicating that it is the second mode of the combustor that is unstable. Also note that there is a low frequency oscillation that brings the system

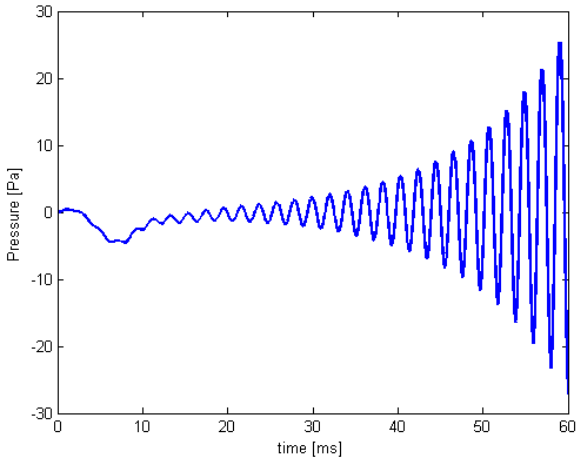

Fig. 5: Response of uncontrolled system to a disturbance in λ_{O_2}.

back to zero, before the high frequency oscillations grows large. This is because the first acoustic mode is stable. If we look back at the experimental results (Figure 1), the unstable frequency differs for the different operating points. This is due to the geometry in the burner, where there exist modes based on the whole combustor length, and on the length of the premixing chamber and burning chamber only. A more advanced model for acoustics will be able to represent this. The growth rate of the instability is dependent on the damping ζ. For $\zeta > 0.039$ the model becomes stable.

F. Scaling

To be able to compare the different manipulated variables available in the system, scaling is necessary. With scaling the process gains from the different manipulators will be comparable. We choose to scale the system from the manipulators influence on ϕ and λ_{O_2}. This ensures that the system is operated close to the operating point it was designed for. The following bounds are used on ϕ and λ_{O_2}

$$|\phi'|_{\max} = 0.05 \qquad \left|\lambda'_{O_2}\right|_{\max} = 0.05.$$

We then use the relations between each of the mass flows and ϕ, λ_{O_2} (equation (19)) to scale each of the mass flows so that they independently cannot violate the bounds on ϕ and λ_{O_2}. This gives $\left|w'_{CH_4}\right|_{\max} = \bar{w}_{O_2}\alpha_0 \left|\phi'\right|_{\max}$, $\left|w'_{CO_2}\right|_{\max} = \left(\frac{\bar{\lambda}_{O_2}}{\alpha_1 M_{CO_2}}\right)^{-1} \left|\lambda'_{O_2}\right|_{\max}$, and $\left|w'_{O_2}\right|_{\max} = \max\{\left(\frac{\bar{\phi}}{\bar{w}_{O_2}}\right)^{-1} |\phi'|_{\max}, \left(\frac{1-\bar{\lambda}_{O_2}}{\alpha_1 M_{O_2}}\right)^{-1} \left|\lambda'_{O_2}\right|_{\max}\}$. The bound on u_c is then dependent on the largest mass flow. Looking at the numerical values for the scaling reveals that this is w'_{CO_2}, resulting in $|u_c|_{\max} = \frac{\left|w'_{CO_2}\right|_{\max}}{\rho_u n_f \pi R^2}$. We then collect all the scaling factors in a scaling vector D_u. If we denote the original system by $\hat{G}$, the scaled system is $G = \hat{G}D_u$. Note here that the actual manipulated variables are the derivatives on the variables we used for the scaling process. Differentiating the variables should have the same effect on all inputs, thus the relation between the variables should still be the same. However this means that the scaling did not have the effect that all inputs are limited to be between -1 and 1.

IV. Model analysis

In this section we will study the input part of the system. The variable we wish to control is the pressure (p'). Other alternatives, for instance Q', are also possible. However, stabilization of p' will lead to stabilization of Q'. Based on the derived model, we will look at bandwith requirements for the injectors, and how close to the flame we have to place the injectors to achieve good control. There are three different mass streams that can be used to manipulate the system. As mentioned earlier it is special for oxy-fuel that the composition of the oxidizer can be changed. We will use the developed model to investigate how the CO_2 stream compares to the other mass flows. It is also possible to use combination of inputs to control the process. Because ϕ, λ, and u_c enters the modelling equations directly and are examples of combinations, we will include these in the analysis. We choose to use the derivatives of the streams as inputs. The resulting model we use for analysis have 6 different inputs , $u = \begin{bmatrix} \dot{u}'_c & \dot{\phi} & \dot{\lambda}_{O_2} & \dot{w}_{CH_4} & \dot{w}_{O_2} & \dot{w}_{CO_2} \end{bmatrix}$.

A. Poles and zeros

The location of the poles and zeros of a plant G gives information about how easy it is to control G. The developed model have a pair of conjugate RHP-poles (right half plane) located at $p = 0.1129 \pm 3.0205i$. To stabilize a plant with RHP-poles, we need to react sufficently fast, and we must require that the closed loop bandwith is larger than $\omega_c > 0.67\left(x + \sqrt{4x^2 + 3y^2}\right)$ for a pair of complex RHP-poles $p = x \pm jy$, [15]. Thus we get a lower bound on $\omega_c = 3564\,\mathrm{rad}/\mathrm{s}$. However, all the inputs except $\dot{u}'_c$ have zeros located close to $z = 750$. RHP-zeros will always imply an inverse response in the time domain, and thus limit the achievable bandwidth. Using a low-frequency performance weight, [15] gives $\omega_c < z/2 = 350\,\mathrm{rad}/\mathrm{s}$ as an upper bound on the achievable bandwith. It is of course impossible to satisfy both of these bounds, which means that this plant is difficult to control. All the inputs also have a set of zeros located at the imaginary axis, which again implies control problems at steady state. A RHP-zero z will give a very small gain at frequencies close to z. Thus, one might consider tight control at frequencies sufficently higher than z. In this case the zero will give a lower bound on the bandwith. By using a performance weight for tight control at high frequencies, [15] gives $\omega_c > 2z = 1500\,\mathrm{rad}/\mathrm{s}$ as a lower bound on the bandwith. As the focus in this application is to reduce high frequency oscillations, it makes sense to use this performance limitation. Thus it is the RHP-poles that determine the limit on lower bandwidth. Conversion to Hz gives $567\,\mathrm{Hz}$ as the bandwith limitation. This is a very high bandwith and might be problematic. In general solenoid valves have been popular for active control of combustion. For instance, the MOOG D633 DDV valve have been used in several experiments, and [16] showed that this valve had a flat frequency response up

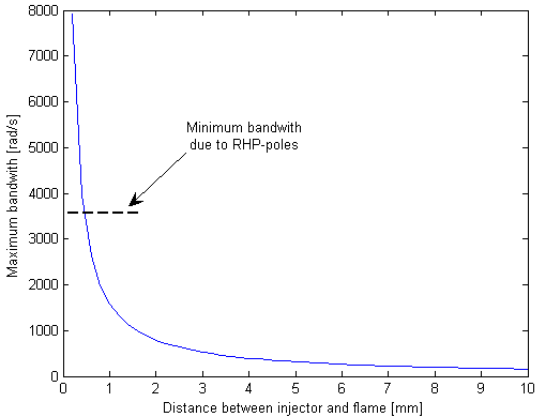

Fig. 6: The bandwith limitation imposed by a time delay due to the distance between injector and flame.

to 380 Hz. An alternative is to use magnetostrictive valves, for instance [17] used a valve from Etrama Products Inc. with a bandwith of 1000 Hz. Thus there should exist valves that are fast enough. Another problem is of course that this limits the complexity of the controller to be used.

B. Time delay

Depending on the location of the injectors, there will be a time delay associated with the transport of input changes to the flame zone, $\tau_c = L_c/\bar{u}$, where L_c is the distance from the injector to the burning zone. The time delay will impose a serious limitation on the achievable bandwith, because every control action will be delayed by τ_c. An upper bound for the achievable bandwith in a plant with a time delay θ is derived in [15] as $\omega_c < 1/\theta$. Figure 6 shows the minimum bandwith requirement as a function of distance between injector and flameholder. As the poles already give a necessary bandwith of $3564\,\mathrm{rad/s}$, there is not much freedom in injector location. To satisfy the bound imposed by the RHP-pole, we need $L_c < 0.5\,\mathrm{mm}$. This is a very difficult requirement to handle, and in practice one will probably have to violate it. A time delay is a nonlinear phenomena, which might lead to oscillations if the design bandwidth of the controller is too high (too large gain). However, since setpoint control is not an objective and there is considerable measurement noise, these oscillations might not be too serious in closed loop operations anyway. An example of control of a conventional combustion process with large time delay can be found in [12].

A problem that might occure when L_c is small, is poor mixing. When using fuel injectors, this have resulted in generation of hot spots on the flame surface, due to pockets of pure fuel entering the flamezone. In additon to hot spots, secondary diffusion flames due to poor mixing where reported in [18]. If using CO_2 injectors for control, the opposite might occur. Pockets of CO_2 might cause the flame temperature to be reduced. However, this is probably not as problematic as the hot spots. Anyway, the injector placement will always be a trade-off between good mixing and problems related to time delay.

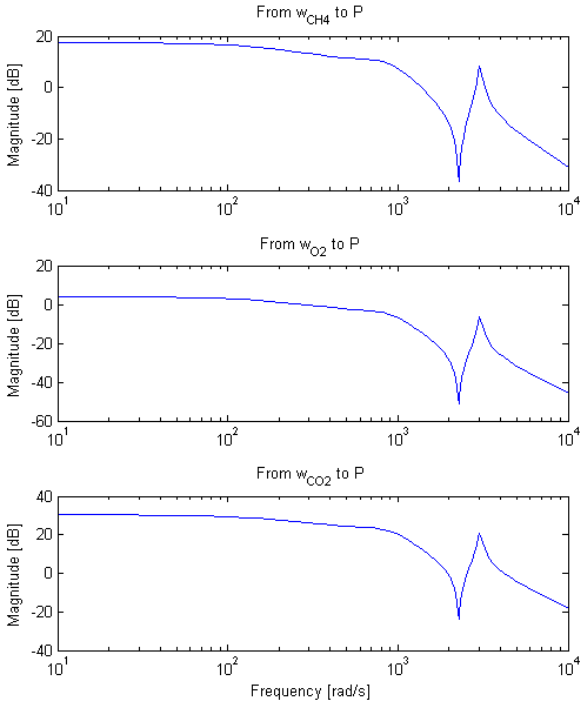

Fig. 7: Bode plots for transfer function between $\dot{w}_{CH_4}$, $\dot{w}_{O_2}$, $\dot{w}_{CO_2}$ and p'

C. Manipulated variables

When the system is scaled as in Section III-F, we can compare the different manipulated variables control authority by investigating their process gain. According to [15] we should choose manipulators with a high gain at frequencies where control is needed. For a system with a single output, comparing the gains give the same results as relative gain array (RGA) analysis. Figure 7 shows a Bode plot for the for the transfer function between mass flows, $\dot{w}_{CH_4}$, $\dot{w}_{O_2}$ and $\dot{w}_{CO_2}$, and the pressure p'. We recognize the RHP-poles and zeros from the sharp peaks in the Bode plots.

The Bode plot shows that the gain is largest for $\dot{w}_{CO_2}$. This indicates that $\dot{w}_{CO_2}$ should be prefered as a manipulated variable over $\dot{w}_{CH_4}$, which is the common manipulated variable in active control of conventional combustion processes. It might seem surprising that $\dot{w}_{O_2}$ has the lowest gain. This is the only variable that can influence both ϕ and λ_{O_2}. However, if we look at equation (19) we see that it enters ϕ and λ_{O_2} with opposite signs. As these variables enter (18) with the same sign, increasing ϕ and λ_{O_2} tend to cancel each other. Why the gain is larger for $\dot{w}_{CO_2}$ can also be understood from the model equations. If we look back at Figure 4 we see that S_u has a much stronger dependance on λ_{O_2} than ϕ. A consequence is that, d_2 is larger than d_1 and when we look at equation (18) we see that these are the constants that decide the gains of the system.

It is also possible to use several injectors simoultanously to control the system. This will result in a much more complex control structure and plant. However, if the gain

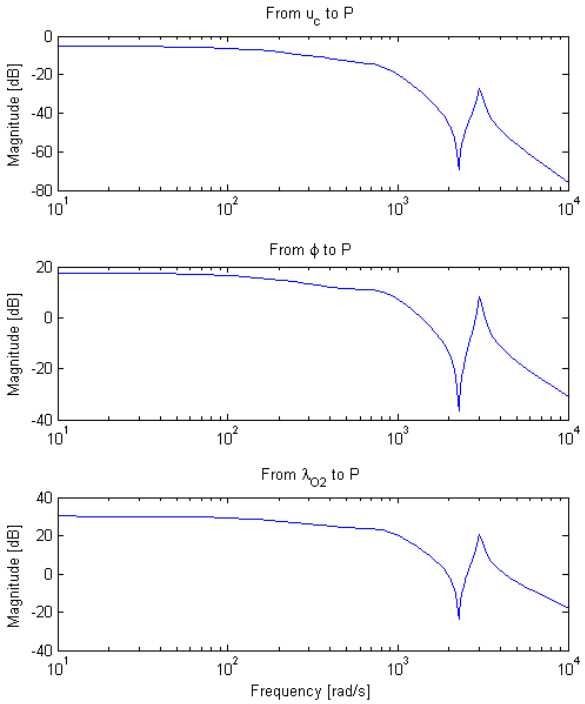

Fig. 8: Bode plots for transfer function between $\dot{u}_c$,$\dot{\phi}$, $\dot{\lambda}_{O_2}$ and p'

from such an input is much higher than for the mass flows, one might consider to use such an input. Examples of such combinations are $\dot{\phi}$, $\dot{\lambda}_{O_2}$, and $\dot{u}_c$. Figure 8 shows the Bode plots for these variables. The only variable that have a gain comparable to $\dot{w}_{CO_2}$ is $\dot{\lambda}_{O_2}$. However, as they are really close, we still prefer $\dot{w}_{CO_2}$ as the controlled variable for the system. It is somewhat surprising that using several injectors do not result in better control. However, other combinations of injectors might perform better than the ones analyzed.

There exist other advantages with using $\dot{w}_{CO_2}$ as the input, which is not revealed by the model. First, oxy-fuel will be used in processes where CO_2 is captured, thus the usage of CO_2 is free. Because we operate at near stoichiometric conditions, the usage of either $\dot{w}_{O_2}$ or $\dot{w}_{CH_4}$ will result in either incomplete combustion, or combustion with excess of oxygen. As both fuel and oxygen costs money, they are less desireable as inputs. Also, usage of CO_2 does not influence the total amount heat produced in the combustion, and will therefore not cause significant fluctuations in power production in for instance a gas turbine.

V. Conclusions

We have presented a linear low order model suitable for active control of oxy-fuel combustion. Analysis on this model shows that a secondary injector modulating a CO_2 stream can perform better than fuel injection, which has been a popular choice for active control of conventional combustion processes. The analysis also show that oxy-fuel combustion is difficult to control. Especially due to high bandwith requirements and transport delays. A natural continuation of this work will be to use the derived model to design a model based controller. Also, the model should be validated with experimental data.

Acknowledgments

The authors gratefully acknowledge Mario Ditaranto at SINTEF Energy Research for helpful discussions, and in particular for assistance in generating the data shown in Figure 4. The Gas Technology Center NTNU-SINTEF and the NFR BIGCO2 project are acknowledged for financial support.

References

[1] O. Bolland and S. Saether, "Comparison of two removal options in combined cycle power plants," *Energy Conversion and Management*, vol. 33, pp. 5–8, 1992.

[2] I. Ulizar and P. Pilidis, "A semiclosed-cycle gas turbine with carbon dioxide-argon as working fluid," *Journal of Engineering for Gas Turbines and Power*, vol. 119, pp. 612–616, 1997.

[3] R. E. Ulfsnes, O. Bolland, and K. Jordal, "Modelling and simulation of transient performance of the semiclosed O_2/CO_2 gas turbine cycle for CO_2-capture," in *Proceedings of ASME TURBO EXPO*, 2003.

[4] D. Snarheim, L. Imsland, R. Ulfsnes, O. Bolland, and B. A. Foss, "Control design for a gas turbine plant with CO_2 capture capabilities," in *Proc. 16th IFAC World Congress, Prague, Czech Republic*, 2005.

[5] L. Imsland, D. Snarheim, B. A. Foss, R. Ulfsnes, and O. Bolland, "Control issues in the design of a gas turbine cycle for CO_2 capture," *International Journal of Green Energy*, vol. 2, no. 2, 2005.

[6] A. M. Annaswamy and A. F. Ghoniem, "Active control of combustion instability: Theory and practice," *IEEE Control Systems Magazine*, vol. 22, pp. 37–54, 2002.

[7] M. Ditaranto and J. Hals, "Combustion instabilities in sudden expansion oxy-fuel flames," *Combustion and Flame*, vol. 146, pp. 439–512, 2006.

[8] L. J. Rayleigh, "The explanation of certain acoustical phenomena," *Nature*, vol. 18, 1878.

[9] S. Candel, "Combustion dynamics and control: Progress and challanges," *Proceedings of the Combustion Institute*, vol. 29, pp. 1–28, 2002.

[10] A. P. Dowling and A. S. Morgans, "Feedback control of combustion oscillations," *Annual review of Fluid Mechanics*, vol. 37, pp. 151–182, 2005.

[11] M. Fleifil, A. Annaswamy, Z. Ghoniem, and A. Ghoniem, "Response of a laminar premixed flame to flow oscillations: A kinematic model and thermoacoustic instability results," *Combustion and Flame*, vol. 106, pp. 487–510, 1996.

[12] J. Hathout, A. Annaswamy, and A. Ghoniem, "Modeling and control of combustion instability using fuel injection," in *Meeting on Active Control Technology*, 2000.

[13] H. A. Nilsen, "Modelling and control of oxy-fuel combustion," Master's thesis, Norwegian university of science and technology, 2006.

[14] A. Annaswamy, M. Fleifil, J. Hathout, and A. Ghoniem, "Impact of linear coupling on the design of active controllers for the thermoacoustic instability," *Combustion, Science and Technology*, vol. 128, pp. 131–180, 1997.

[15] S. Skogestad and I. Postlethwaite, *Multivariable Feedback Control Analysis and Design*, 2nd ed. Wiley, 2005.

[16] D. Bernier, S. Ducruix, F. Lacas, and S. Candel, "Transfer function measurements in a model combustor: Application to adaptive instability control," *Combustion, Science and Technology*, vol. 175, pp. 993–1013, 2003.

[17] S. S. Sattinger, Y. Neumeier, A. Nabi, B. T. Zinn, D. J. Amos, and D. D. Darling, "Sub-scale demonstration of the active feedback control of gas-turbine combustion instabilities," *Journal for Engineering for Gas Turbines and power*, vol. 122, pp. 262–268, 2000.

[18] J. P. Hathout, M. Fleifil, A. M. Annaswamy, and A. F. Ghoniem, "Active control using fuel-injection of time-delay induced combustion instability," *AIAA Journal of Propulsion and Power*, vol. 18, pp. 390–399, 2002.